EVOLUTION OF MATERIAL LINE IN TURBULENT CHANNEL FLOW

Takahiro Tsukahara, Kaoru Iwamoto[*], Hiroshi Kawamura
Department of Mechanical Engineering,
Tokyo University of Science
Yamazaki 2641, Noda-shi, Chiba 278-8510, Japan
tsuka@rs.noda.tus.ac.jp, kawa@rs.noda.tus.ac.jp

ABSTRACT

The Lagrangian evolution of passive material lines in a turbulent channel flow is studied through direct numerical simulation (DNS). A series of DNS has been performed for the friction Reynolds number of $Re_\tau = 80$–395 with various initial condition of lines. The present study reveals that fine-scale phenomenon, in particular the near-wall coherent structure, makes a significant contribution to the turbulent mixing. The line stretching rate, normalized by the local Kolmogorov time, is less dependent on the height nor the Reynolds number except the one in the wall vicinity . It is shown qualitatively by visualization of a cross-sectional flow that a streamwise vortex and a bursting process cause the intensive stretching and the anisotropy of the line deformation.

INTRODUCTION

An important feature of turbulence is its ability to transport and mix fluid effectively. Evolutions of material objects in turbulence are of intrinsic interest, and their stretching properties reflect a high potential of mixing by turbulence. A material object is defined as any line, surface or volume that always consists of the same material points or fluid particles. The stretching and the deformation of a material line by turbulence provide important consequences, such as, stretching of a vortex line in an inviscid fluid, and a motion of a polymer as drag-reducing surfactant. Constant-property surfaces of temperature or of other passive scalars are material surfaces in case of the negligible molecular diffusivity compared to the turbulent mixing. Hence, passive material objects have been extensively studied by a number of authors as one of the most fundamental topics. Their deformation is of practical importance in flows accompanied by diffusion of chemical reactants in the turbulence combustion or of pollutant in the environment.

Batchelor (1952) was the first to simplify the analysis of the finite-sized lines and surfaces to that of infinitesimal elements in his study of the homogeneous isotropic turbulence. It has been theoretically and numerically confirmed by Goto & Kida (2003), and by references therein, that the total length $\mathcal{L}(t)$ of a material line increases exponentially in time. Recently, the evolution of infinitesimal material line has been investigated experimentally by Guala *et al.* (2006) with a focus on the effect of vorticity and strain. The stretching rate, if normalized by the Kolmogorov time τ_η,

$$\gamma \equiv \frac{\mathrm{d}}{\mathrm{d}t}\log \mathcal{L}(t) \qquad \Big(\because \mathcal{L}(t) = \mathcal{L}_0 \exp(\gamma t)\Big) \tag{1}$$

is found to be independent of the Reynolds number Re. This supports the conjecture that small-scale elementary vortices contribute to exponential evolution in material objects. On the other hand, it is emphasized in Goto & Kida (2003) that a correct stretching rate cannot be obtained correctly by random selection of line elements in the flow volume (the Batchelor's assumption). This implies that material-line elements can never be statistically equivalent even in the homogeneous turbulence. Moreover, Goto & Kida (2005) reported that the stretching rate of the finite-sized material line in the homogeneous turbulence depends on Re; i.e., it is larger at a higher Re. This dependence is caused by the combined effect of various-scale eddies; the folding of a material line by large eddies and the stretching by small eddies.

Much attention was paid to the material line (or line element) in the homogeneous isotropic turbulence as mentioned above. To the authors' knowledge, no study to date has been done to verify the exponential stretching of a material line in a wall-bounded shear flow. We are interested, in particular, in the relationship between the stretching of the material line and coherent structures near a wall. In the wall turbulence, the scale of vortical structures is known to range over several orders from the near-wall fine-scale structure to the large-scale one in the outer region, cf. Robinson (1991). In recent years, the direct numerical simulation (DNS) of the turbulent channel flow, which is a canonical case in the wall turbulence, has become an important research tool in studying the physics of the turbulent structure. However, the influence of the multi-scale eddies and the near-wall viscous effect on the material-line evolution are not yet understood.

The objective of this work is to perform the simulation of the material line released in the channel flow through DNS, and to examine the physical mechanism of strong mixing and of stretching of material objects in the wall turbulence. The visualizations reveal clearly that the stretching depends on its initial condition, i.e. direction and height from the wall, in addition to the Reynolds number. This paper deals with the performance of the numerical simulation and obtained statistics such as the stretching rate and the fractal dimension, with emphasis on these parameters.

NUMERICAL PROCEDURE

The Lagrangian velocity data of a material object are obtained from DNS of a fully-developed turbulent channel flow, as given in Fig. 1. The mean flow is driven by the uniform pressure gradient in the x direction. The periodic

[*]Present affiliation: Department of Mechanical Systems Engineering, Tokyo University of Agriculture and Technology, Nakacho 2-24-16, Koganei, Tokyo 184-8588, Japan. e-mail: iwamotok@cc.tuat.ac.jp

Table 1: Numerical parameters of DNS and Eulerian statistics: Re_τ=$(u_\tau\delta/\nu)$, Reynolds number; L_i, computational domain size; N_i, number of grids points; Δi, spatial resolution; Δt, time step; $\Delta_{\mathcal{L}}$, threshold length of line segment; η, local Kolmogorov length; τ_η, of local Kolmogorov time.

Re_τ	$L_x \times L_y \times L_z$	$N_x \times N_y \times N_z$	Δx^+	$\Delta y^+_{\min}$–$\Delta y^+_{\max}$	Δz^+	Δt^+	$\Delta^+_{\mathcal{L}}$	$\eta^+_{\min}$–$\eta^+_{\max}$	$\tau\eta^+_{\min}$–$\tau\eta^+_{\max}$
80	$12.8\delta \times 2\delta \times 6.4\delta$	$256 \times 96 \times 256$	4.00	0.111–3.59	2.00	0.0128	1.00	1.77–2.86	3.12–8.20
180	$12.8\delta \times 2\delta \times 6.4\delta$	$256 \times 128 \times 256$	9.00	0.200–5.93	4.50	0.0360	2.25	1.57–3.67	2.47–13.5
395	$12.8\delta \times 2\delta \times 6.4\delta$	$512 \times 192 \times 512$	9.88	0.148–6.51	4.94	0.0395	2.47	1.48–4.55	2.12–20.7

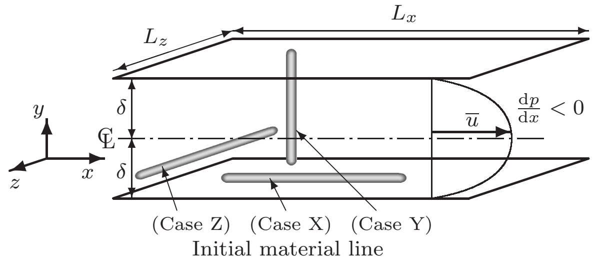

Figure 1: Configuration of a channel flow and material lines. The initial material line is straight, and parallel to the streamwise coordinate in Case X; the wall-normal one, Case Y; or the spanwise one, Case Z.

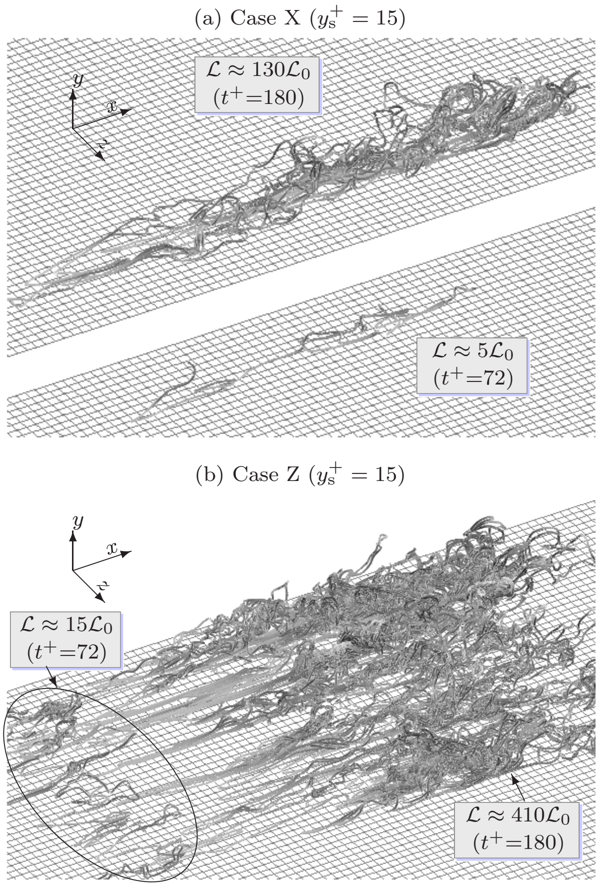

Figure 2: Consecutive snapshots of of a material line as it evolves until t^+=180 in the turbulent channel flow at Re_τ = 180: from the initial height $y_s^+ = 15$. Instantaneous length at each time is also shown; the initial length $\mathcal{L}_0$ is equal to 6.4δ. The mean flow direction is from bottom-left to top-right. The grid width of a horizontal plane indicates $20\eta(y_s)$. For Case Z (b), two lines at the different times show their actual relative location.

boundary conditions are imposed in the x and z directions and the non-slip condition is applied on the walls. The fundamental equations are the continuity and the Navier-Stokes equations. For the spatial discretization, the finite difference method is adopted. Further details of the numerical scheme for the flow field can be found in Abe *et al.* (2004). The Eulerian statistics calculated from the present DNS are in good agreement with the previous works (Abe *et al.*, 2004; Tsukahara *et al.*, 2005).

A passive material line is expressed numerically by a set of a number of advecting infinitesimal particles. Once the channel flow simulation has reached equilibrium, we start with the particle tracking. The particle equation of motion for individual point on a material line is advected by the local velocity as

$$\frac{\mathrm{d}}{\mathrm{d}t}\mathbf{x}_\mathrm{p}(t) = \mathbf{u}(\mathbf{x}_\mathrm{p}(t), t), \qquad (2)$$

with $\mathbf{x}_\mathrm{p}$ the particle position and $\mathbf{u}$ the fluid velocity. The perfect elastic collision is adopted on the walls. For practice, however, no particle reaches the wall surfaces, because the wall-normal velocity tends to be zero in the close vicinity of the wall. A segment between two neighboring particles generally growths in time. To express a line smoothly by a set of particle points, all segments must be kept short enough compared to the Kolmogorov scale η. When a segment exceeds a given threshold $\Delta_{\mathcal{L}}$ ($\approx O(\eta_{\min})$) as time elapses, a new particle is inserted at the center of the segment. The time step for Eq. (2) is also small enough ($\Delta t \ll \tau_\eta$).

We report here several cases of the different Reynolds numbers of Re_τ = 80, 180 and 395 (based on the friction velocity u_τ and the channel half width δ). The computational conditions are presented in Table 1. Some important Eulerian statistics are also shown for comparison. The superscript of $^+$ indicates a non-dimensional quantity scaled by the viscous wall units. In order to calculate the evolution of a material line for a long enough time, number of released particles has increased up to 6×10^7 in the present simulation.

RESULT AND DISCUSSION

We have carried out simulations for three cases in which a material line is initially aligned with either of the three coordinate axes (streamwise, wall-normal or spanwise direction) as shown in Fig. 1. Hereafter, the case of the initial material line parallel to x axis is called "Case X"; those parallel to y and z are "Case Y" and "Case Z", respectively.

Temporal Evolution of Material Line

Several snapshots of typical temporal evolutions of a material line at the time of t^+ = 72 and 180 are shown in Figs. 2–4. In order to study the effect of the distance from the wall, the material lines are released at $y_s^+ = 15$ and 180

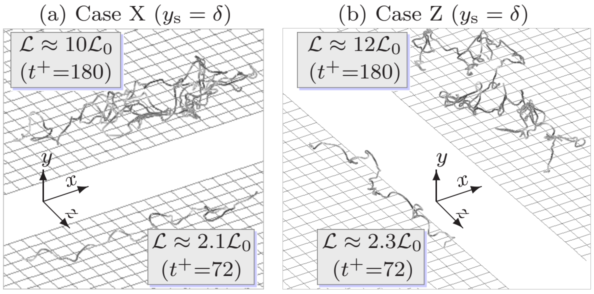

Figure 3: Same as Fig. 2 but for $y_s = \delta$.

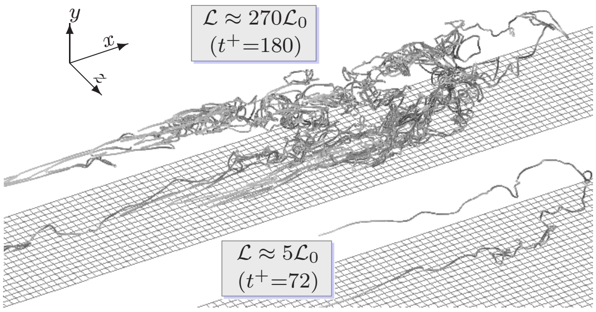

Figure 4: Same as Fig. 2 but for Case Y ($\mathcal{L}_0 = 2\delta$). The grid width of a horizontal plane is same with that of Fig. 2.

for $Re_\tau = 180$, which correspond to $y_s = 0.083\delta$ and δ, respectively (here, y_s is referred to as an initial height of a material line for Case X and Z). A material-line length $\mathcal{L}$ is initially $\mathcal{L}_0$ at t^+=0 and increases up to $410\mathcal{L}_0$ (Case Z, $y_s = 15$) at $t^+ = 180$, in which the mean flow has passed by the computational domain (1.3 wash-out time). It is observed in these figures that the material line is strongly deformed by turbulence. The deformations of the $y_s^+ = 15$ lines is clearly more rapid than those of the $y_s = \delta$ lines. The grid width of the horizontal plane shown in Figs. 2 and 3 indicates 20 times Kolmogorov lengthscale η at y_s. Note that both η and τ_η are minimum in the wall region and increase in the outer region. The lines seem to be convoluted by the Kolmogorov-scale vortex at each height. The lower and higher-Re_τ simulations (visualization not shown) also imply that the deformation is governed by the smallest-scale eddies. This is consistent with the result in homogeneous isotropic turbulence by Goto & Kida (2003). They reported that the average curvature of deformed lines is $O(10\eta)$ irrespective of the Reynolds number.

If we compare the deformed lines of Cases X and Z in the early stage (at t^+=72), the line of Case Z from $y_s^+ = 15$ is found to be stretched faster than the one of Case X from the same height, as shown in Fig. 2. It is well known that quasi-streamwise vortices dominate in this region ($10 < y^+ < 30$). In addition, the evolution of the material line at $y_s^+ = 15$ in Fig. 2 (b) is qualitatively similar to that of a vortex line detected by the conditional sampling technique though the simulation (see Kim & Moin, 1986). Hence, it can be suggested that the material-line deformation is closely related to the near-wall coherent vortical structures. In Fig. 3, on the other hand, there is no significant difference of the line deformation between Cases X and Z in the channel center, where the turbulent mixing is nearly isotropic.

Figure 4 shows that a growing line initially normal to the wall (Case Y) is deformed rapidly into a complicated structure in the both upper- and lower-side near-wall regions.

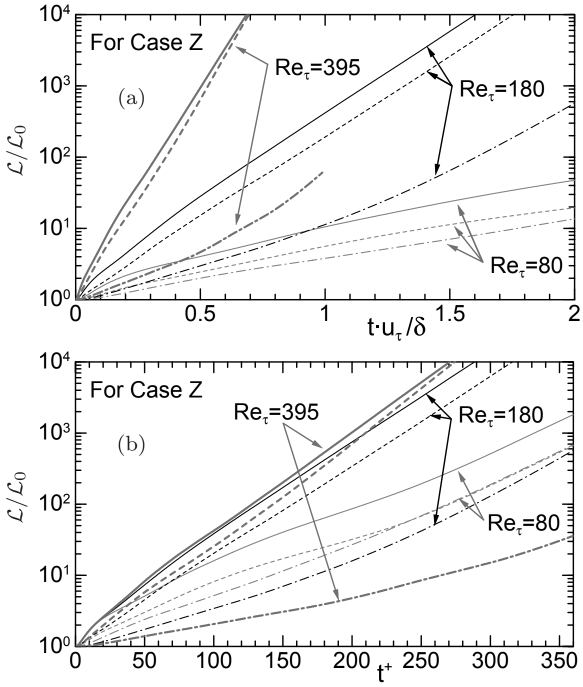

Figure 5: Line stretching in the channel flow: the various conditions in Caes Z are plotted versus time normalized by the outer-scale variables (a), or by the wall units (b). The length of the line is normalized by the initial length, Initial height is $y_s^+ = 5$, - - - -; $y_s^+ = 15$, ——; and $y_s = \delta$, — · —. The results are averaged over 16 lines.

The mean velocity gradient $\partial\overline{u}/\partial y$ deforms the line into an elongated shape in the streamwise direction. It, however, results in a linear growth but not an exponential one. As pointed out in the introduction, the exponential growth is brought into a material object evolution by elementary vortices. Most part of elongation takes place near the walls, where the vortical structures are smaller than ones of the outer region. Actually, the total length of Case Y increases as rapid as that of the Case Z ($y_s^+ = 15$), as discussed later.

Stretching Rate

To calculate the statistical quantities, the averaging is performed over at least 128 realizations for Case Y; and 16 realizations for the other cases, in which the initial length of a material line for Case X and Z is relatively long. The mean material-line length is plotted as a function of nondimensional time for various Reynolds numbers in Fig. 5. The straight line in this semi-logarithmic scale indicates that the length increases exponentially in time. When the time is normalized by the outer timescale, the growth of a material line becomes faster at higher Reynolds numbers. We note here that a small-scale phenomenon should be dominant for the growth of the line, so that the growth rate is scaled more suitably by the viscous timescale. The plot against t^+ indeed shows better scaling, as seen in Fig. 5 (b).

The stretching rate, γ (defined in Eq. (1)), is plotted for $Re_\tau = 180$ in Fig. 6. On the figure one may notice that: (i) The transient evolution of γ for an early period t^+=0–100 shows remarkable dependences on the height from the wall and on the direction of the material line. (ii) In the channel central region (Fig. 6 (d)), less noticeable dependence is observed on the initial direction as anticipated from

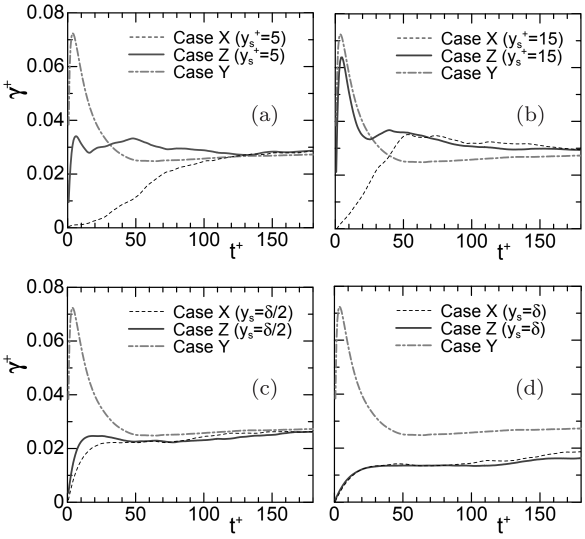

Figure 6: Average stretching rate γ of a material line as a function of time t for $Re_\tau = 180$. Both γ (defined in Eq. (1)) and t are normalized by the wall units. (a) $y_s^+ = 5$ for Case X and Z, (b) $y_s^+ = 15$, (c) $y_s = \delta/2$, (d) $y_s = \delta$.

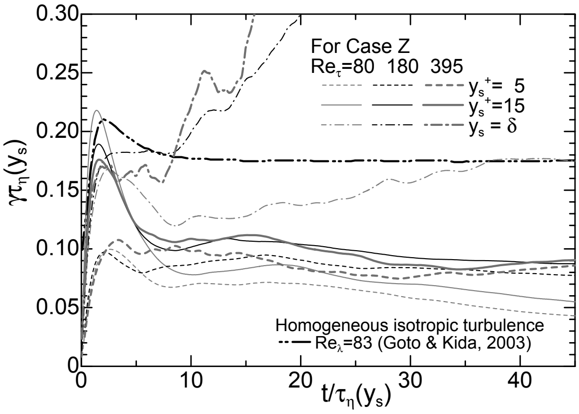

Figure 7: Average stretching rate γ of a material line: γ and time are normalized by the local Kolmogorov time $\tau_\eta(y_s)$.

the visualization described above. (iii) After a transient period, $t^+ > 100$, γ^+ tends to be close to a steady-state value of 0.029 at $Re_\tau = 180$; 0.022, at $Re_\tau = 80$; and 0.033, at $Re_\tau = 395$ (see Fig. 6 (a–c) but figure not shown for the latter two Re_τ). With scaling by the minimum Kolmogorov time $\tau_{\eta_{\min}}$, the steady-state stretching rate settles down around γ=$0.07\tau_{\eta_{\min}}^{-1}$ irrespective of Re. (iv) The line of Case Y and the lines of Cases X and Z from the near-wall region become fully developed at an earlier time ($t^+ \approx 120$) than the one in the outer region ($t^+ > 360$, not shown here). (v) The large γ^+, i.e. the enhanced stretching, is observed in Case Y and Case Z with $y_s^+ = 15$, both exhibit almost the same variation in the early stage (see Fig. 6 (b)).

The latter two observations confirm that the line of Case Y is stretched especially in the near-wall region as well as the $y_s^+ = 15$ line for Case Z. It can be inferred that the coherent structure in the near-wall region induces the enhanced stretching of the material lines in the turbulent channel flow.

The time and the stretching rate of Fig. 7 are normalized by the local Kolmogorov time at its own initial height. For the first some Kolmogorov times, the curves except for the

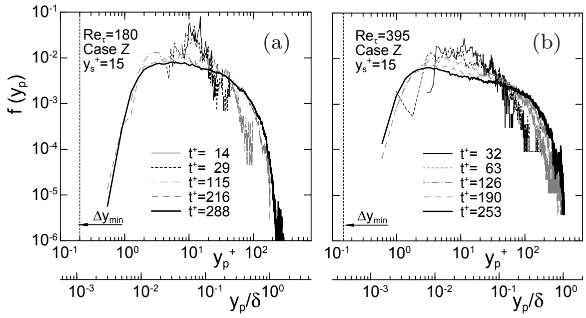

Figure 8: P.d.f. of the height of points on a material line *versus* time: for $y_s^+ = 15$ (Case Z) at $Re_\tau = 180$ (a) and 395 (b). The height of the lowest grid $\Delta y_{\min}$ is also shown for comparison.

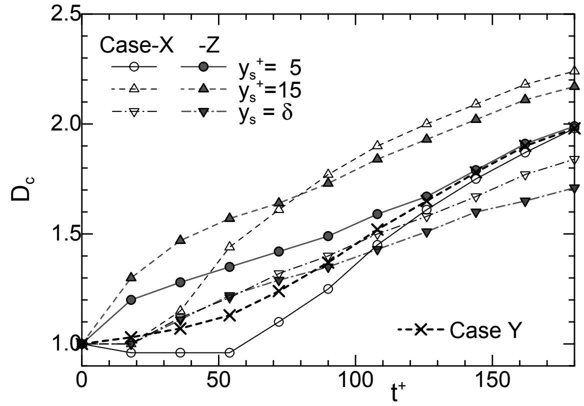

Figure 9: Correlation dimension of a deformed line as a function of time at $Re_\tau = 180$. The results are averaged over 16 lines.

line of $y_s^+ = 5$ are better correlated irrespective of the initial height and of the Reynolds number. For comparison, a typical result in the homogeneous isotropic turbulence by Goto & Kida (2003) is also shown in Fig. 7. Moreover, it can be found that $\gamma\tau_\eta$ in the channel flow is comparable to that in homogeneous turbulence, especially for the early times.

It is interesting to note that the $\gamma\tau_\eta$ for $y_s = 5$ is remarkably small in the early stage (see $0 < t/\tau_\eta < 5$ in Fig. 7), whereas the values of $y_s = 5$ and 15 are not significantly different after 10 Kolmogorov times. The probability density functions of the height of points on a material line measured from the lower wall are plotted in Fig. 8 for various times. It should be noticeable that the peak of p.d.f. for the developed line arises at the wall vicinity (y^+=3–5), not at the enhanced-stretching region (y^+=15). This implies that the once stretched line in the buffer region is blown down by the sweep motion and accumulated in the vicinity of the wall.

Fractal Dimension

In this section we compute a correlation dimension D_c of a material line in order to quantify the line-deformation speed and the complexity of turbulent mixing. The correlation dimension we considered here is a correlation exponent ν_c obtained by the algorithm of Grassberger and Procaccia (1983). The exponent is closely related to the fractal dimension, and its computation is considerably easier than another method to calculate the fractal dimension. In this method, we measure the spatial correlation of points lying

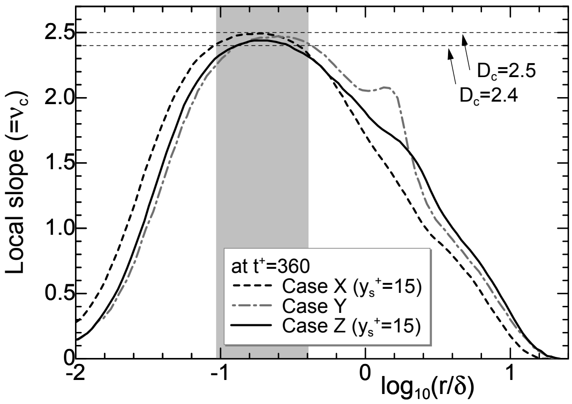

Figure 10: Local slope of the correlation integral, cf. Eq. (4), in order to evaluate the correlation dimension of a fully-developed material line by GP algorithm: at t^+=360, for $Re_\tau = 180$. Gray-colored band indicates the 10–20 times Kolmogorov-scale range: $10\eta_{\min}$, at the left-side demarcation of the band; $20\eta_{\max}$, at the right-side one.

on a material line with the correlation integral $C(r)$, which is defined according to

$$C(r) = \lim_{N\to\infty} \frac{1}{N^2} \sum_{i,j=1, i\neq j}^{N} H\Big(r - \big|\mathbf{x}_\mathrm{P}(i) - \mathbf{x}_\mathrm{P}(j)\big|\Big). \quad (3)$$

Here, N is the number of points on the material line, H the Heaviside function, and $\mathbf{x}_\mathrm{P}(i)$ the position vector of i-th particle. Local slope of the correlation integral as a function of the distance r indicates the ν_c. A certain range of r, in which $C(r)$ can be represented by a power law

$$C(r) \propto r^{\nu_\mathrm{c}} \quad \left(\nu_\mathrm{c} = \frac{\mathrm{d}\log C(r)}{\mathrm{d}\log r}\right), \quad (4)$$

is called 'scaling range'. The constant ν_c corresponds to D_c.

Figure 9 shows the dimension of the material line as a function of time. The D_c becomes larger than topological dimension ($D = 1$), thus suggesting some kind of self-similarity in the deformed line. In all cases except for the early period of Case X ($y_\mathrm{s}^+ = 5$), the D_c increases with time. The gradient of the incrementation depends on the initial condition of the line, while not for $t^+ > 120$.

The result of the correlation integral is shown at $t^+ = 360$ in Fig. 10. The correlation dimension of the fully-developed line in any case reveals its asymptotic value of about 2.5, which agrees well with those obtained by Mandelbrot (1975) and Sreenivasan (1991). They report that, for passive scalars of unit Schmidt number, the fractal dimension of a scalar interface is 2.3–2.5 independent of flow configuration as long as the flow is fully turbulent. It appears from Fig. 10 that there exists a scaling range (shown with a gray band in the figure) over which the fractal dimension is D_c = 2.4–2.5. The scaling range roughly accords with the diameter of the fine-scale eddies in the turbulent channel flow (Tanahashi *et al.*, 2004). For very small distances of $r/\delta \ll 0.1$, the data for $C(r)$ deviate from a power law, which was to be expected because the behaviour for $r \ll \eta$ is not chaotic.

Infinitesimal-line-element growth: Stretched Factor

In addition to the finite-sized material-line simulation presented as above, we also executed DNS with respect to an infinitesimal line-element stretching. To examine the

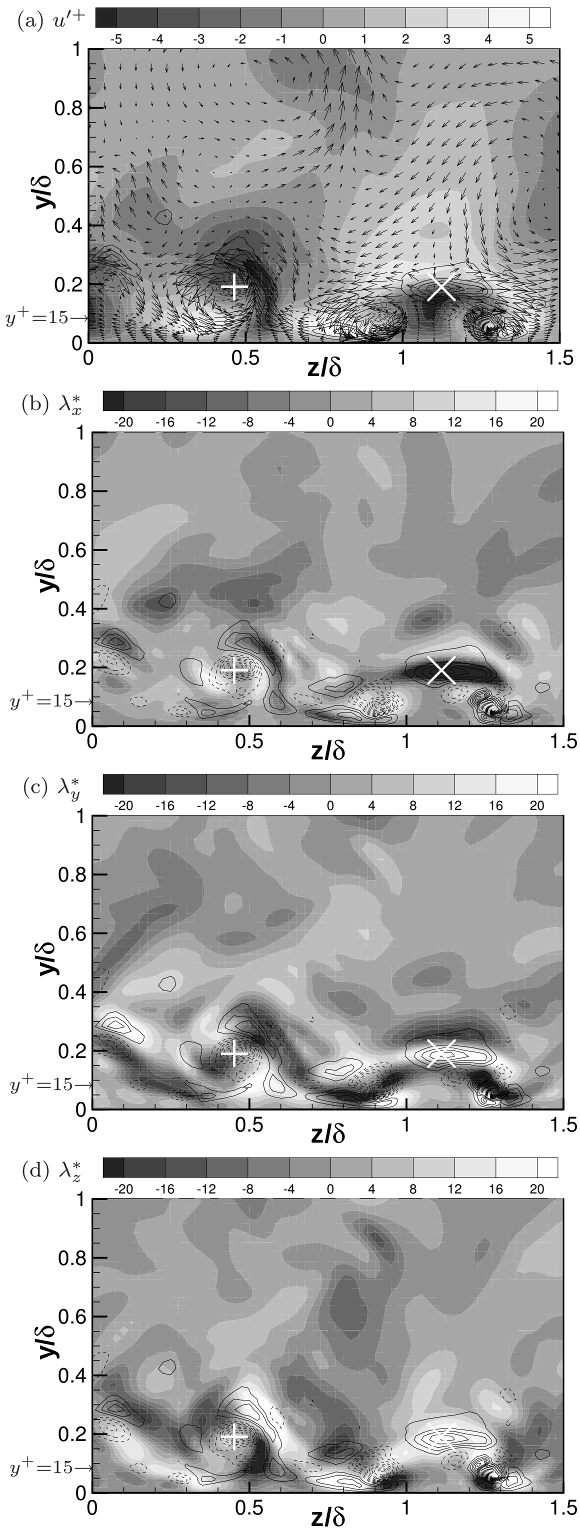

Figure 11: Contours of an instantaneous flow field and stretched-factor distributions in a (z, y) cross section: vector in (a) shows (w', v') velocity; color contours (a) streamwise velocity fluctuation u'^+, (b) streamwise component of the stretched factor λ_x^*, (c) wall-normal component λ_y^*, and (d) spanwise component λ_z^*; isoline contours II'^+ (from −0.3 to 0.1 with increments of 0.02, but line of 0.0 is not shown). Solid and dashed lines represent positive and negative quantities, respectively. White markers indicate the center of the quasi-streamwise vortex (+), and the location of the burst associated with Q2/Q4 event (×).

contribution of the coherent structures upon the enhanced stretching, it is convenient to consider line elements at several points. Here, we address the issue of the relationship between the structures and the stretched factor λ_i (defined as follows) of line elements:

$$\lambda_i = \frac{1}{\Delta t} \log \frac{|\delta x_i(\Delta t)|}{|\delta x_i(0)|} \quad (5)$$

$$= \frac{1}{\Delta t} \log \left| \frac{\partial \mathbf{u}'}{\partial x_i} \Delta t + \mathbf{e}_i \right|, \quad (6)$$

where δx_i denotes a line-element length. The λ_i represents the exponential rate of separation of two infinitesimally close flow fields: its positive value notes an exponential growth of the i-direction line.

In Fig. 11, we show the flow field on a cross-section of arbitrarily chosen coherent structures which are located at the near-wall region. A quasi-streamwise vortex and a burst are detected by the second invariant II'^+ of deformation tensor. Contours of λ_x, λ_y and λ_z are given in Fig. 11 (b)–(d), where the symbols denoting the vortex and the burst are also shown. Figures 11 (c) and (d) show that the intensified growths of the spanwise line element and of the wall-normal one, i.e. $\lambda_z \gg 0$ and/or $\lambda_y \gg 0$, take place at the burst event and around the quasi-streamwise vortex. On the other hand, as for the λ_x in Fig. 11 (b), a negative region corresponds to the burst. These results are consistent with the high stretching rates in Case Y or Case Z ($y_s^+ = 15$) and with the low rate in Case X, as discussed above.

In this paper, the material-line evolution are described in order to study the turbulent mixing. It is also important to predict the turbulent dispersion of a scalar contaminant or heat. Le & Papavassiliou (2005) investigated the dispersion of the scalar emitted from a line source in the turbulent channel flow at various Prandtl numbers. They reported that the enhancement of turbulent dispersion is attributed to the large-scale structure in the outer layer. However, due to the exponential growth, it is difficult to simulate material-line dispersion for a long enough time to capture the large-scale motion. With the use of recent supercomputers it should be possible to study the long-time evolution of a material line and surface. This kind of study is planned for the future.

CONCLUSION

We performed DNS of the turbulent channel flow in which the motion of a material line had been calculated. The stretching rate and the fractal dimension of the material line are analysed with emphasis on the dependence on the initial conditions.

When normalized by the minimum Kolmogorov time, the steady-state stretching rates are scaled well for the present Reynolds number range irrespectively of the initial condition, which is in agreement with previous work on homogeneous isotropic turbulence. However, the stretching rate of $\gamma = 0.07\tau_{\eta_{\min}}^{-1}$ is smaller than that ($\gamma = 0.17\tau_{\eta_{\min}}^{-1}$) of the homogeneous turbulence by Goto & Kida (2003), since the Kolmogorov scale changes with respect to the height from the wall. Both visualizations and statistical results show that the enhanced stretching is closely associated with the fine-scale coherent structures in the near-wall region, except for the wall vicinity ($y^+ \leq 5$). The material lines normal to the flow direction are stretched well in the buffer region. Their fractal dimensions increase remarkably with time, but they do not exceed $D_c = 2.5$ even if the lines are fully developed.

ACKNOWLEDGEMENTS

The first author (T.T.) is supported by Japan Society for the Promotion Science Fellowship (18-81). The present computations were performed with use of the supercomputing resources at Information Synergy Center of Tohoku University. This work was conducted in Research Center for the Holistic Computational Science (Holcs) supported by MEXT.

REFERENCES

Abe, H., Kawamura, H., and Choi, H., 2004, "Very large-scale structures and their effects on the wall shear-stress fluctuations in a turbulent channel flow up to $Re_\tau = 640$," *Tran. ASME I: J. Fluids Eng.*, Vol. 126, pp. 835–843.

Batchelor, G. K., 1952, "The effect of homogeneous turbulence on material lines and surfaces," *Proc. R. Soc. Lond. A*, Vol. 213, pp. 349–366.

Goto, S., and Kida, S., 2003, "Enhanced stretching of material lines by antiparallel vortex pairs in turbulence," *Fluid Dyn. Res.*, Vol. 33, pp. 403–431.

Goto, S., and Kida, S., 2005 "Reynolds number dependence of material line and surface stretching in turbulence," *Proc. 4th Int. Symp. on Turbulence and Shear Flow Phenomena*, J.A.C. Humphrey *et al.*, ed., pp. 95–98.

Grassberger, P., and Procaccia, I., 1983, "Measuring the strangeness of strange attractors," *Physica D*, Vol. 9, pp. 189–208.

Kim, J., and Moin, P., 1987, "The structure of the vorticity field in turbulent channel flow. Part 2. Study of ensemble-averaged fields," *J. Fluid Mech.*, Vol. 162, pp. 339–363.

Le, P. M., and Papavassiliou, D. V., 2005, "Turbulent dispersion from elevated line sources in channel and Couette flow," *AIChE J.*, Vol. 51, pp. 2402–2414.

Mandelbrot, B. B., 1975, "On the geometry of homogeneous turbulence, with stress on the fractal dimension of the iso-surfaces of scalars," *J. Fluid Mech.*, Vol. 72, pp. 401–416.

Robinson, S. K., 1991, "Coherent motions in the turbulent boundary layer," *Annu. Rev. Fluid Mech.*, Vol. 23, pp. 601–639.

Sreenivasan, K. R., 1991, "Fractals and multifractals in fluid turbulence," *Annu. Rev. Fluid Mech.*, Vol. 23, pp. 539–600.

Tanahashi, M., Kang, S.-J., Miyamoto, T., Shiokawa, S. & Miyauchi, T., 2004, "Scaling law of fine scale eddies in turbulent channel flows up to $Re_\tau = 800$," *Int. J. Heat and Fluid Flow*, Vol. 25, pp. 331–340.

Tsukahara, T., Seki, Y., Kawamura, H., and Tochio, D., 2005, "DNS of turbulent channel flow at very low Reynolds numbers," *Proc. 4th Int. Symp. on Turbulence and Shear Flow Phenomena*, J.A.C. Humphrey *et al.*, ed., pp. 935–940.